

# PCCP

Accepted Manuscript



This is an *Accepted Manuscript*, which has been through the Royal Society of Chemistry peer review process and has been accepted for publication.

*Accepted Manuscripts* are published online shortly after acceptance, before technical editing, formatting and proof reading. Using this free service, authors can make their results available to the community, in citable form, before we publish the edited article. We will replace this *Accepted Manuscript* with the edited and formatted *Advance Article* as soon as it is available.

You can find more information about *Accepted Manuscripts* in the [Information for Authors](#).

Please note that technical editing may introduce minor changes to the text and/or graphics, which may alter content. The journal's standard [Terms & Conditions](#) and the [Ethical guidelines](#) still apply. In no event shall the Royal Society of Chemistry be held responsible for any errors or omissions in this *Accepted Manuscript* or any consequences arising from the use of any information it contains.

# Structural characterization of eutectic aqueous NaCl solutions under variable temperature and pressure conditions

A.-A. Ludl, L. E. Bove, A. M. Saitta, M. Salanne, T. C. Hansen, C. L. Bull, R. Gaal and S. Klotz

Received Xth XXXXXXXXXX 20XX, Accepted Xth XXXXXXXXXX 20XX

First published on the web Xth XXXXXXXXXX 200X

DOI: 10.1039/b000000x

The structure of amorphous NaCl solutions produced by fast quenching is studied as a function of pressure, up to 4 GPa, by combined neutron diffraction experiments and classical molecular dynamics simulations. Similarly to LiCl solutions the system amorphizes at ambient pressure in a dense phase structurally similar to the e-HDA phase in pure water. The measurement of the static structure factor as a function of pressure allowed to validate a new polarizable force field developed by Tazi *et al.*, 2012, never tested at non-ambient conditions. We infer from simulations that the hydration shells of Na<sup>+</sup> cations form well defined octahedra composed of both H<sub>2</sub>O molecules and Cl<sup>-</sup> anions at low pressure. These octahedra are gradually broken by the seventh neighbour moving into the shell of first neighbours yielding an irregular geometry. In contrast to LiCl solutions and pure water, the system does not show a polyamorphic transition under pressure. This confirms that the existence of polyamorphism relies on the tetrahedral structure of water molecules which is broken here.

## 1 Introduction

Electrolytic aqueous solutions, such as LiCl and NaCl water solutions, are key systems for the understanding of the behaviour of water molecules under the influence of Coulomb forces and they are of key relevance in diverse fields of science ranging from geology to energy technology. LiCl solutions have been studied in depth since the early 1970s in the attempt to address the thermodynamic and structural properties of water in the deep undercooled regime<sup>2–4</sup>, the stability of which is promoted by the addition of ions in water. Furthermore, the properties of solvated ions in solutions have been addressed extensively<sup>5–7</sup> as they are crucial for the understanding of a variety of chemical and biological processes. The concept of structure-breaking and structure-making, where ions are supposed either to disrupt the hydrogen-bond network or to form ionic hydration structures in water, has been widely used to provide at least a qualitative understanding of the effect of ions on the structure of water<sup>6,8,9</sup>. Detailed knowledge of the non-equilibrium phase diagram of common electrolyte aqueous solutions, such as LiCl, NaCl and KCl-water solutions, and of the structural properties of the hydration shell of their ions has thus been achieved, at least at ambient and moderate ( $p < 2$  kbar) pressures. A variety of techniques have been employed to this end, including X-ray diffraction, extended X-ray absorption fine-structure spectroscopy (EXAFS), neutron diffraction with isotopic substitution, and simulation techniques.<sup>1,4–7,9–14</sup>

More recently the high-pressure phase diagram of the prototypical LiCl-solutions has been investigated.<sup>15–17</sup> Evidence has

been provided for the existence of high-pressure ice phases including considerable amounts of salt in their lattice.<sup>15</sup> Furthermore, a polyamorphic transition under high pressure has been observed.<sup>16</sup> The phenomenon of polyamorphism is the coexistence of two amorphous states of different density and local arrangement of molecules. In particular a polyamorphic transition has been observed between a high-density relaxed state, produced by cooling the eutectic solution<sup>18</sup> at ambient pressure, and a very high density state, produced by annealing the solution under high pressure. This last state has been shown to be very stable up to multi-GPa pressures, and to be the amorphous precursor of the salty ice VII lattice formed upon annealing to room temperature under high pressure<sup>15</sup>. Of note is the fact that the Li<sup>+</sup> ion is octahedrally coordinated at high-pressure in both the amorphous and the crystalline phase. The observed polyamorphic transition is due to the change of the coordination\* around the Li<sup>+</sup> ion from four-fold at ambient pressure to six-fold at high pressure.<sup>16</sup> Whether the existence of a polyamorphic transition is a common feature of electrolytic aqueous solutions and whether it is linked to the polyamorphic transition observed in pure water<sup>19</sup>, as suggested by recent Raman studies<sup>20</sup>, still remains to be established.

In this paper we investigate the high-pressure metastable phase diagram of NaCl aqueous solutions close to the eutectic composition using both high-pressure neutron diffraction and molecular dynamics simulations, along the thermodynamic paths indicated on the metastable phase diagram of LiCl solu-

\*The coordination number of Li ion is the number of water molecules or chlorine ions populating the first shell of solvation.

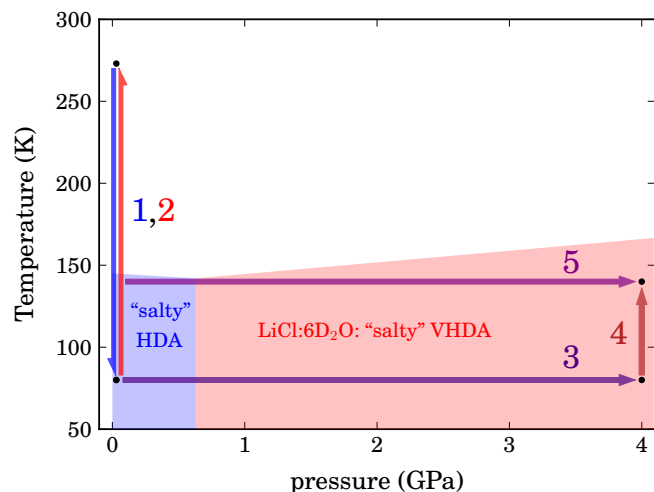


**Fig. 1** The thermodynamic path along which  $\text{NaCl} \cdot 10.2\text{D}_2\text{O}$  has been studied, by neutron diffraction and MD simulations. The coloured regions indicate the boundaries of amorphous phases of previously studied  $\text{LiCl} \cdot 6\text{D}_2\text{O}$ .<sup>16</sup> Arrows: 1: hyper-quench at ambient pressure, 2: warming at ambient pressure (Figure 3), 3: compression at 80 K (Figure 4), 4: annealing at 4 GPa (MD and neutron diffraction experiments), 5: compression at 140 K (MD simulations only).

tion in Figure 1.  $\text{NaCl}$  is biologically and geochemically more important than  $\text{LiCl}$  and the existence of new amorphous and crystalline phases of  $\text{NaCl}$  water solutions could be of high relevance for the physics of both living organisms and celestial icy bodies<sup>21,22</sup>. Up to now  $\text{NaCl}$  di-hydrate is the only known solid compound formed by the  $\text{NaCl}$  and  $\text{H}_2\text{O}$  system. No phase transition in the solid state has been detected, in contrast to the  $\text{LiCl}$  and  $\text{H}_2\text{O}$  system where several hydrates are formed, depending on the salt concentration and pressure conditions.

The essential building blocks of the  $\text{NaCl} \cdot 2\text{H}_2\text{O}$  structure are the octahedra about each sodium ion and the tetrahedra about each water molecule. While  $\text{Na}^+$  ions are octahedrally coordinated in the crystalline phase, they show large variations in the coordination number in solution, ranging from 4 to 6, depending on the anion and the salt concentration.<sup>5,23,24</sup>

## 2 Methods

### 2.1 Sample preparation

We prepared sodium chloride aqueous solutions,  $\text{NaCl} \cdot R\text{D}_2\text{O}$  and  $\text{NaCl} \cdot R\text{H}_2\text{O}$ , by mixing de-hydrated  $\text{NaCl}$  salt with pure (99.75 %)  $\text{H}_2\text{O}$  and  $\text{D}_2\text{O}$  respectively. Compositions close to the eutectic, *i.e.*  $R = 9.7$  in  $\text{H}_2\text{O}$  and  $R = 10.2$  in  $\text{D}_2\text{O}$ , were chosen in order to maximize the amorphisation ability of the solution<sup>2</sup>. The amorphous phase was produced by fast quenching of the solution to liquid nitrogen temperature

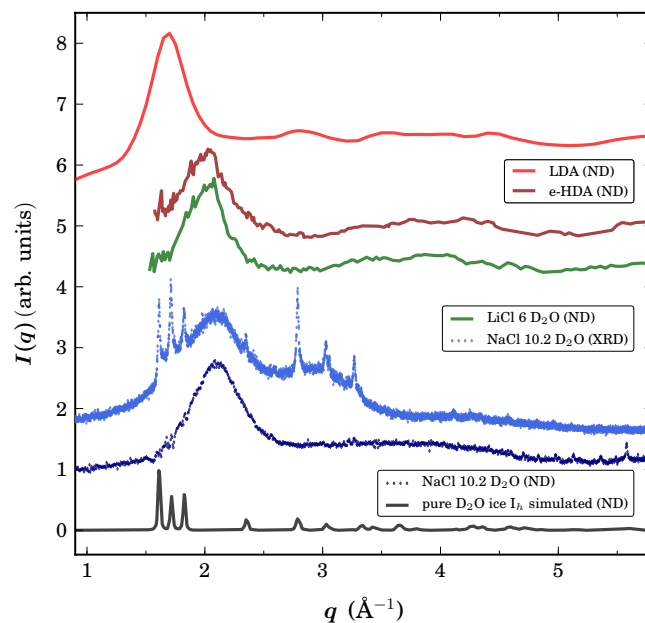


**Fig. 2** Diffraction patterns of amorphous aqueous phases at low pressure. From bottom up: Fullprof<sup>25</sup> simulation of the neutron diffraction spectrum of pure  $\text{D}_2\text{O}$  ice  $I_h$  powder,  $\text{NaCl} \cdot 10.2\text{D}_2\text{O}$  neutron pattern measured on  $\text{D}_2\text{O}$  at ILL (100 mbar),  $\text{NaCl} \cdot 10.2\text{D}_2\text{O}$  X-ray pattern measured at IMPMC ( $10^{-3}$  mbar),  $\text{LiCl}$  solution neutron data<sup>16</sup> (1 bar), pure water e-HDA<sup>26</sup> at 0.18 GPa and LDA<sup>19</sup> at 0.1 GPa. The position of the maximum of the first diffraction peak of  $\text{NaCl} \cdot 10.2\text{D}_2\text{O}$  is at  $2.1 \text{ \AA}^{-1}$  and for  $\text{LiCl} \cdot 6\text{D}_2\text{O}$  it is at  $2.015 \text{ \AA}^{-1}$ . The data show that both  $\text{NaCl}$  and  $\text{LiCl}$  solutions at ambient pressure closely resemble the high pressure amorphous phase of pure water (e-HDA), rather than the low density amorphous phase (LDA).

(77 K) with an estimated cooling rate of  $10^4 \text{ K s}^{-1}$ . This high quenching rate was obtained by spraying micro droplets, diameter  $\approx 10$  to  $30 \mu\text{m}$ , of the solution on a cold plate maintained at 77 K under vacuum. Details of the quenching device will be given elsewhere<sup>27</sup>.

The thin film of quenched solution was reduced to fine powder, recovered under  $\text{N}_2$  vapour, and stored in plastic containers filled with liquid nitrogen. Roughly 1 g of powder were produced for each quenching procedure. In order to check the quality of amorphization, a small amount of quenched solution was systematically recovered and studied *ex situ* at ambient pressure by X-ray diffraction with a commercial XPERT powder X-ray diffractometer, equipped with a low-temperature Anton Paar chamber. The sample holder made of nickel plated copper was cooled to  $\approx 80 \text{ K}$  with liquid nitrogen and the temperature of the sample during the transfer did not exceed 95 K. The diffractometer has an incident wavelength of  $\lambda = 1.5418 \text{ \AA}$  ( $\text{Cu K}\alpha$ ). During the measurement the X-ray source and the detector were set up in  $\theta/2\theta$  geometry.

Figure 2 shows an example of the X-ray diffraction pat-

tern of hyper-quenched  $\text{NaCl} \cdot 10.2\text{D}_2\text{O}$  solution at 80 K and  $10^{-3}$  mbar. As readily seen from the diffraction pattern the sample is largely amorphous. The crystalline contribution of ice  $I_h$  accounts for less than 5 % of the total intensity. The samples with the largest fraction of amorphous material were selected for the neutron diffraction experiments.

For high pressure experiments in the Paris-Edinburgh cell the sample powder was compacted to spherical pellets using a dedicated press operating at liquid nitrogen temperature up to 2 kbar. The packing density of the pellet is estimated to be 90 %. The pellets were maintained at 77 K by storage in a liquid nitrogen dewar.

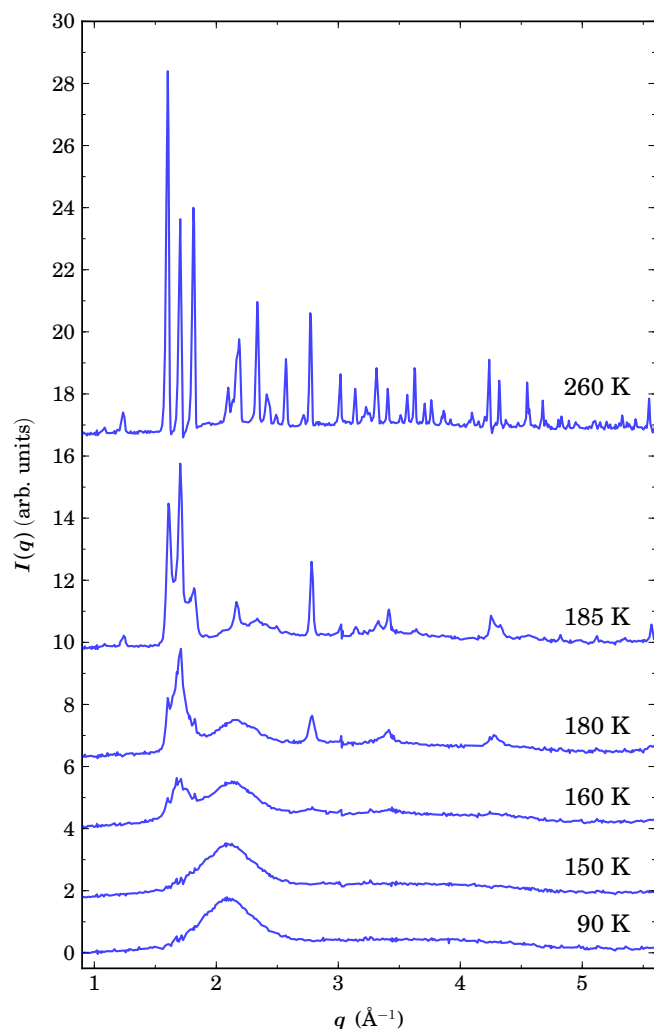


**Fig. 3** Neutron diffraction pattern of amorphous  $\text{NaCl} \cdot 10.2 \text{D}_2\text{O}$  measured at D20 (ILL) while heating at  $p = 100$  mbar. First “cubic ice” starts growing at 160 K, which then transforms into hexagonal ice at 185 K. Sodium chloride dideuterate appears at 185 K. At 260 K the spectrum shows a mixture of ice  $I_h$  and sodium chloride dideuterate.

## 2.2 Neutron diffraction experiments

The ambient pressure study was carried out on the high-intensity two-axis diffractometer D20<sup>28</sup> at the high-flux reactor of the Institut Laue-Langevin (ILL, Grenoble, France) using a wavelength of 1.87 Å (with average resolution of  $\delta d/d = 3 \cdot 10^{-3}$ ). The sample environment was a helium flow cryostat pre-cooled at 80 K, with a pressure of approximately 100 mbar of helium exchange gas. The powder sample was loaded into a cylindrical vanadium cell of 6 mm diameter kept in liquid nitrogen. During this experiment three solutions of different concentrations close to the eutectic one were measured. The one with the highest proportion of amorphous material was chosen for detailed analysis. Diffraction patterns were collected during warming from liquid nitrogen to room temperature in steps of approximately 20 K. Once the temperature was stabilized, data were collected for 40 minutes below 160 K and 20 minutes above 165 K. Empty vanadium cell, empty cryostat, and vanadium standard measurements were performed to normalize the spectra.

In order to remove the background contribution from the cryostat, the data were reduced using the formula

$$I_{\text{corr}}(q) = \frac{I_{\text{mes}}(q) - I_{\text{bg}}(q) - t(q) (I_{\text{ec}}(q) - I_{\text{bg}}(q))}{I_{\text{van}}(q) - I_{\text{bg}}(q) - t_{\text{van}} (I_{\text{ec}}(q) - I_{\text{bg}}(q))} \quad (1)$$

where  $I_{\text{mes}}$  is the intensity scattered by the sample,  $I_{\text{bg}}$  is the intensity scattered by the empty cryostat,  $I_{\text{ec}}$  the intensity scattered by the empty can,  $I_{\text{van}}$  is the intensity scattered by the can filled with vanadium standard,  $t_{\text{van}} = 0.96$  is the transmission of vanadium and  $t$  is the  $q$  dependent transmission of the sample ( $0.77 \leq t(q) \leq 0.78$ ). The division to correct for detector efficiency was done at the beamline. An example of collected data after background correction is shown in Figure 2, alongside the X-ray diffractogram and equivalent spectra collected for  $\text{LiCl} \cdot 6\text{D}_2\text{O}$  solution<sup>16</sup>.

Figure 3 shows neutron structure factors recorded during the annealing of our sample. The spectrum at 90 K corresponds also to the blue data points in Figure 2. At low temperature the sample produced by hyper-quenching is largely amorphous. The reflections of the remaining crystalline component (see suppl. material for the raw data) correspond all to ice  $I_h$  by comparison with simulations, though with significant texture. To remove these peaks from the data, they were fitted individually with pseudo-Voigt functions to the pattern at 90 K and subtracted from the data collected during annealing to give the patterns in Figure 3. For the subtraction we took into account the  $q$  and temperature dependence of the Debye-Waller factor.

$$I_{\text{am}}(q, T) = I_{\text{corr}}(q, T) - \frac{DW(q, T)}{DW(q, T_0)} \cdot I_{h,\text{fit}}(q, T_0) \quad (2)$$

where  $I_{\text{am}}$  is the structure factor of the amorphous part,  $I_{h,\text{fit}}$  is a fit of the peaks of ice  $I_h$  in the data, and

$T_0 = 80$  K. The Debye-Waller factor is given by  $DW(q, T) = D_0 \exp(-\frac{2}{3}q^2 \langle u^2(T) \rangle)$  for ice  $I_h$  with  $D_0$  being a constant and a linear estimate for the average mean square displacement  $\langle u^2(T) \rangle$  was interpolated from the experimental data in Pektrenko and Whitworth, 1999<sup>29</sup> (p. 24).

By integrating the intensities derived from these fits we find the sample to be 92% amorphous, *i.e.* the crystalline component is 8% of the total volume. The neutron experiment provides evidence that the crystalline contamination occurs during the hyperquenching process and not during loading of the sample, since the measured ice peaks correspond to deuterated ice  $I_h$ .

Upon warming “cubic ice” nucleates at 160 K and it gradually transforms into hexagonal ice. At about 185 K the amorphous  $\text{NaCl} \cdot 10.2\text{D}_2\text{O}$  solution dissociates into pure hexagonal ice and sodium chloride dideuterate. This behaviour mirrors that of lithium chloride solutions, as discussed in Elarby-Aquizerat *et al.*<sup>30</sup>.

The high-pressure diffraction experiment was carried out at the time-of-flight PEARL beamline of the ISIS Facility pulsed neutron source in Didcot (United Kingdom)<sup>31</sup>. The pellets of pre-compressed powder (see Section 2.1 for details) were split into two hemispheres and a small piece of lead was placed in between them to serve as a pressure calibrant<sup>32</sup>. The reassembled pellet was subsequently loaded into pre-cooled null-scattering titanium-zirconium ( $\text{Ti}_{0.677}\text{Zr}_{0.323}$ ) encapsulated gasket (Klotz, 2012<sup>33</sup> ch. 2, p. 24) at 80 K. The sample-gasket assembly was placed in pre-cooled sintered diamond anvils under liquid nitrogen, which were clamped before insertion into a pre-cooled V3 Paris-Edinburgh (PE) press. The initial sample volume was approximately  $40 \text{ mm}^3$ . A liquid nitrogen cryostat was used in this experiment to cool the whole PE cell. The details of the cryogenic setup are described in Klotz, 2012<sup>33</sup> (ch. 11, p. 141–145). The vanadium standard for this experiment was a sphere of vanadium of the same size as the sample, which was loaded into the gasket and the PE cell in the same setup as the sample at ambient pressure and ambient temperature ( $I_{van}$  in equation 1).

The gasket was sealed by applying a load of 80 kN on the anvils. The first scan was recorded at the initial load, corresponding to 0.5 GPa on the sample. Then pressure was increased in steps of about 0.5 GPa up to 4 GPa. Thereafter the sample was annealed up to 150 K at 4 GPa with a warming rate of  $\approx 20 \text{ K hr}^{-1}$ . The load was reduced at 185 K in order to maintain the pressure close to 4 GPa on the sample. Data were collected continuously, with time slices of 1 hour being summed for the points along the thermodynamic path followed during the experiment as shown in Figure 1.

The diamond anvils strongly scatter neutrons and their contribution to the pattern needs to be subtracted, as described by equation 1 which also takes into account detector efficiency

via vanadium calibration. This is not a trivial task in measurements involving the PE cell since the background depends on the anvils’ orientation in the beam. Furthermore, the diamond peaks shift during compression, mainly because the anvils move closer together. The intensity  $I_{ec}$  measured with an empty gasket mounted between the PE anvils at ambient pressure in the cryostat has to be shifted, to take into account the angular shift due to this displacement. We shifted  $I_{ec}$ , the empty gasket measurement at ambient pressure, by the median shift between the diamond peaks positions fitted for each pressure and the fitted positions at ambient pressure. The term  $I_{bg}$  in equation 1, which corresponds to the scattering by the sample environment, was negligible here compared to the other terms. The quality of the subtracted data can be appreciated in Figure 4 where the corrected spectra for representative pressure points are reported.

This compressed sample also contains a fraction ( $\approx 10\%$ )

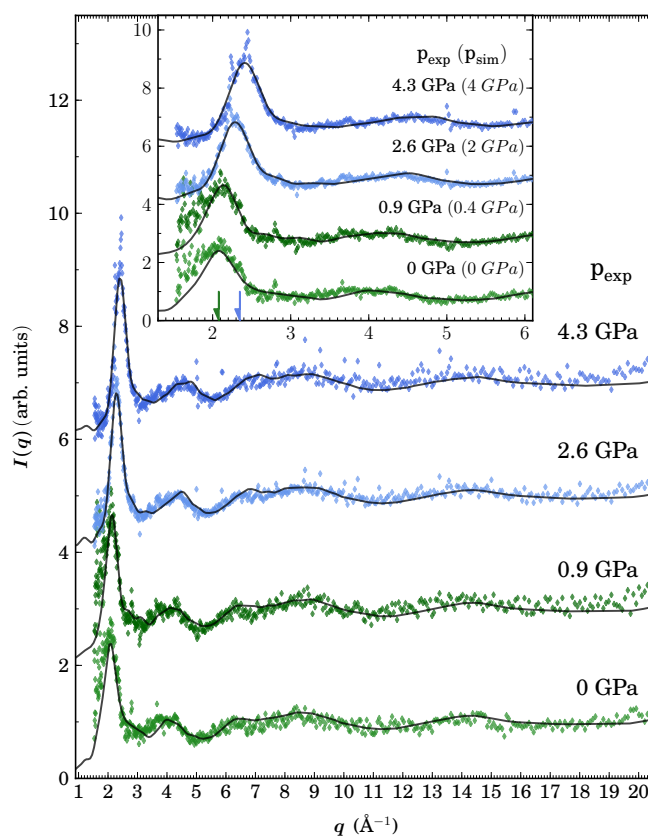


**Fig. 4** Neutron diffraction pattern upon compression of amorphous  $\text{NaCl} \cdot 10.2\text{D}_2\text{O}$  at 80 K. Points are experimental data collected on PEARL (ISIS, UK) and lines are structure factors from MD simulations. The inset shows details for  $q$  in the range of  $1$  to  $6 \text{ \AA}^{-1}$ . The positions of the maxima of the first diffraction peak at  $0 \text{ GPa}$  ( $2.1 \text{ \AA}^{-1}$  in green) and at  $4 \text{ GPa}$  ( $2.35 \text{ \AA}^{-1}$  in blue) are indicated by arrows along the  $q$  axis in the inset.

of hexagonal ice visible in the spectra as sharp peaks. This part transforms during compression and its peaks shift, therefore the crystalline contribution has not been subtracted, unlike the ambient pressure data. In fact compression induces amorphisation of the crystalline part into an HDA phase, which recrystallizes around 2 GPa in the ice VIII phase<sup>34</sup>.

### 2.3 MD simulations

In order to obtain detailed structural information, such as coordination numbers of atomic species or partial radial distribution functions (RDFs)<sup>35</sup>, for the multicomponent system studied here, it is necessary to perform time consuming isotopic substitution experiments. Alternatively, we used molecular dynamics simulations, for which the computed total structure factors and densities were validated against the available experimental data, to derive information on the partial structural correlations. Furthermore, MD simulations yield some quantities, such as the angular distribution functions, which are not available otherwise. MD simulations of the sodium chloride aqueous solution were performed on a cubic box containing 510 water molecules and 51 ion pairs ( $\text{Na}^+$  and  $\text{Cl}^-$ ). The calculations were done using the CP2K 2.2.141 simulation package<sup>36</sup>. The polarizable force field of Dang and Chang was used for water<sup>37</sup>, together with a recently developed polarizable model for the ions<sup>1</sup>. In this model the induced dipoles account for many-body electrostatic effects and are obtained at each MD step by minimizing the polarization energy (with a tolerance of  $10^{-7}$ ). The long-range charge-charge, charge-dipole and dipole-dipole terms were computed using a dipolar Ewald sum<sup>38,39</sup>. The system was simulated in the canonical ensemble (NVT), the temperature being controlled using a Nosé-Hoover thermostat with a time constant of 1 ps.

The simulation cell was initially equilibrated in the liquid phase at a temperature of 300 K and experimental density. It was quenched to 80 K by successive steps of 20 K. A compression was then made, by reducing the box size from 25.725 to 22.7 Å in steps of 0.2 Å. The final pressure was 7.2 GPa. The thermodynamic trajectories followed are shown in Figure 1. At each point the system was simulated for 400 ps, where a 1 fs time step was used in the liquid (above 160 K) and 2 fs in the amorphous domain.

The RDFs, noted  $g_{AB}(r)$ , where  $A$  and  $B$  are two (possibly identical) chemical species provide the probability of finding one specimen of species  $B$  at a distance  $r$  from a specimen of species  $A$ <sup>35</sup>. In our system, which contains 4 species, 10 different RDFs can be calculated. The most relevant ones are shown in Figure 5.  $g_{\text{OO}}$  probes the changes in the water structure,  $g_{\text{ONa}}$  describes the hydration of sodium and  $g_{\text{NaCl}}$  characterizes ion pairing.

Coordination numbers of atoms of species  $B$  in a given shell of neighbours around species  $A$  are calculated by integrating

O–O		Cl–H	
pressure (GPa)	$r_2$ (Å)	pressure (GPa)	$r_2$ (Å)
0.0	3.075	0.0	2.9
0.4 to 1.0	3.025	0.4	2.8
2.0 to 2.4	2.975	1.0 to 2.0	2.75
3.0 to 4.5	2.925	2.4 to 5.0	2.65
5.0 to 7.2	2.875	5.4 to 7.2	2.6

**Table 1** The cut-off radii  $r_2$  for O–O and Cl–H pairs used to calculate coordination numbers, decrease as pressure increases.

$g_{AB}$  over the  $r$  range of the corresponding shell:

$$N_{AB}(r) = 4\pi\rho_B \int_{r_1}^{r_2} dr r^2 g_{AB}(r) \quad (3)$$

A shell is therefore defined by two cut-off distances  $r_1$  and  $r_2$ . For the first neighbour shell,  $r_1$  is set to 0 and  $r_2$  is taken as the first minimum of the corresponding RDF. For Na–O pairs the choice, 3.1 Å, was straightforward as the position of the minimum does not change with pressure. For Na–Cl pairs 3.3 Å was chosen for the whole range of pressures as the best compromise since the minimum is affected non monotonically by pressure for  $p > 3$  GPa. For O–O and Cl–H pairs this minimum shifts to smaller distances when pressure increases, the chosen values are given in Table 1. Average coordination numbers  $N_{\text{OO}}$ ,  $(N_{\text{NaO}} + N_{\text{NaCl}})$ ,  $(N_{\text{ClNa}} + N_{\text{ClH}})$  are reported in Figure 6. Using the same cutoffs the distribution of coordination of Na with Cl and O has been calculated for the compression at 80 K (Figure 7). The lateral panels in figure 7 show the distributions of  $N_{\text{NaO}}$  and  $N_{\text{NaCl}}$  at 80 K for 0 and 5.4 GPa.

The angular distribution function  $P(\theta)$  of O–O–O in the first shell was computed as

$$P(\theta) = \frac{1}{N_{\text{angles}}} \times \left\langle \sum_{i \in A} \sum_{j \in A \setminus \{i\}} \sum_{k \in A \setminus \{i, j\}} \delta(r_{ij} \leq r_2) \delta(r_{ik} \leq r_2) \delta(\theta_{jik} - \theta) \right\rangle \quad (4)$$

and is reported in panel 4 of Figure 5.

The Ashcroft-Langreth partial structure factors  $S_{ij}^{\text{AL}}(q)$  and the total structure factor  $S(q)$  are given by

$$S_{ij}^{\text{AL}}(q) = 1 + 4\pi(c_i c_j)^{\frac{1}{2}} \int_0^\infty dr r^2 \frac{\sin(qr)}{qr} (g_{ij}(r) - 1) \quad (5)$$

$$S(q) = \sum_{i, j} b_i b_j (c_i c_j)^{\frac{1}{2}} S_{ij}^{\text{AL}}(q), \quad (6)$$

where  $c_i$  is the concentration of species  $i$  and  $b_i$  its scattering length. The total structure factors at each pressure point reported in Figure 4, were computed using the ISAACS program following equations 5 and 6.<sup>40</sup>

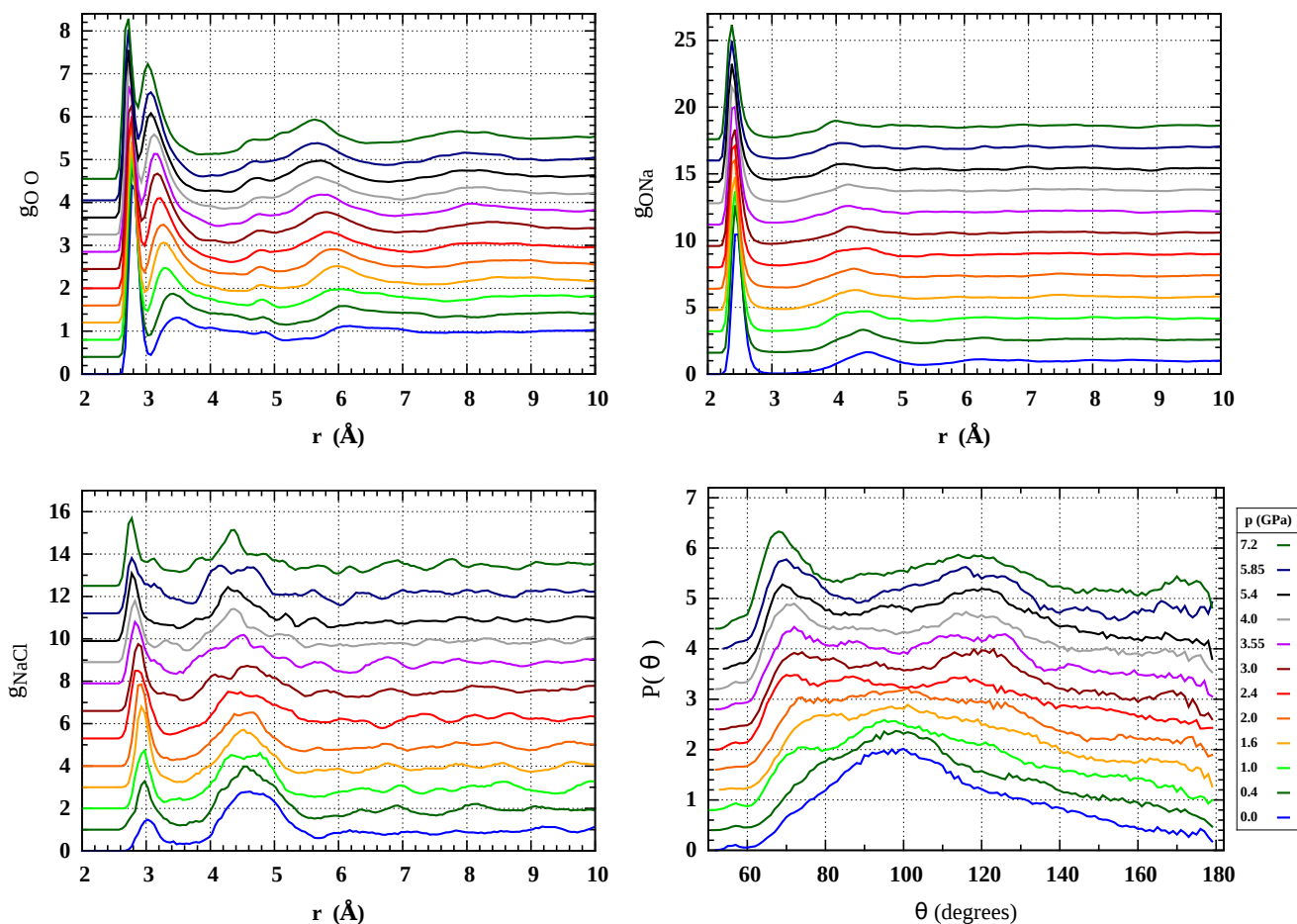


**Fig. 5** Evolution of RDFs  $g_{OO}$ ,  $g_{ONa}$ ,  $g_{NaCl}$  and the angular correlation function  $P(\theta)$  of O-O-O for amorphous  $\text{NaCl} \cdot 10.2\text{D}_2\text{O}$  solution during compression at 80K. In  $g_{OO}$  the second peak shifts toward the first, although the minimum remains more pronounced than during the transition of HDA to VHDA in pure water. In  $g_{ONa}$  the second peak flattens with increasing pressure. In  $g_{NaCl}$  the first peak increases indicating that ions tend to have counterions in their shell of first neighbours at higher pressures. The evolution of  $P(\theta)$  shows that the tetrahedral geometry of the water network is progressively distorted during compression.

### 3 Results and Discussion

The present set of experiments shows that amorphous  $\text{NaCl} \cdot 10.2\text{D}_2\text{O}$  can be produced by a fast quenching method. The system has been investigated by X-ray and neutron scattering under thermal annealing at ambient pressure and at high pressure (4 GPa), and under compression up to 4 GPa at 80 K (Figure 1). The measured structure factor shows that amorphous  $\text{NaCl} \cdot 10.2\text{D}_2\text{O}$  is stable up to about 185 K at ambient pressure as described in Section 2.2. The structure of the quenched solution, shown in Figure 2, is in a dense form much more similar to the relaxed high density phase of pure water (e-HDA), than to its low density phase (LDA) produced by similar hyperquenching techniques. This is also the case for concentrated LiCl solutions<sup>16</sup>, and is a consequence of the electrostrictive effect of sodium and lithium cations on wa-

ter molecules. The usual tetrahedral coordination of water molecules, which is characteristic of the low density phases such as LDA and ice I, is highly distorted by the presence of ions in a way which is similar to the effect of pressure<sup>6,8,9</sup>. It has been previously shown that salt inclusion in solid water, both in the amorphous water network or in the crystalline ice lattice, is possible in dense phases only<sup>14,17,41</sup>.

The behaviour of our  $\text{NaCl} \cdot 10.2\text{D}_2\text{O}$  solution upon annealing at ambient pressure is analogous to that of LiCl solutions. For these solutions of concentration in the vicinity of the metastable eutectic concentration<sup>4</sup>, it has been observed that the water in excess is segregated in small clusters of most likely pure water (or lower concentration solution), dispersed in a vitreous matrix at the eutectic (or higher) concentration<sup>17,41</sup>. These clusters are smaller than the critical ice nucleation cluster. Upon annealing they amorphize as LDA

which in turn transforms to a cubic ice phase at 160 K<sup>9,42</sup>. At about 190 K the cubic ice phase transforms to hexagonal ice. The absence of peaks associated with hydrates or salts below 190 K, indicates that the vitrified solution matrix remains metastable until the concentrated metastable liquid segregates into pure hexagonal ice and a salt hydrate<sup>17,30</sup>.

Upon compression at 80 K and annealing under high pressure the structure densifies continuously, in contrast to pure water where a stepwise change in the density was recorded due to the transformation of LDA into HDA at 0.55 GPa<sup>43,44</sup>. In the present case the position of the first diffraction peak shifts continuously from 2.08 Å<sup>-1</sup> at low pressure to 2.35 Å<sup>-1</sup> at 4 GPa, and no other modification is observed in the static structure factor. No evidence for a transition in local structure and density<sup>†</sup> was observed in the recorded NaCl solution spectra and in our simulations. The structure factor changes continuously upon isothermal compression at 80 K and 140 K, and upon annealing from 80 K to 140 K under high pressure (see suppl. material). Furthermore, the enthalpy trend calculated in our MD simulations along isothermal compression at both 80 K and 140 K, also confirms the absence of a transition in the amorphous system (see suppl. material). This is at variance with the behaviour of LiCl:6D2O solution in which a transition from HDA to VHDA is observed during compression at 138 K and during isochoric annealing at 2 GPa<sup>16</sup>. Finally, the distribution of first neighbours around the cation, which was used to identify the observed transition from 4-fold to 6-fold coordination in amorphous LiCl solutions, is changing smoothly with pressure here, as discussed in the following. Thus we find no evidence for polyamorphism in our sodium

chloride samples, in contrast to the lithium chloride case.

It is noteworthy that the total structure factors extracted from simulations match the experimental ones very well, as shown in Figure 4. The force fields of references<sup>1,37</sup> had only been tested under ambient pressure previously, the agreement observed here for both the structure factor and the density shows that they are remarkably transferable to high-pressure conditions. The ability to reproduce the diffraction patterns allows us to extract additional information on the structure of the compound from our simulations.

The calculated  $g_{OO}$  (Figure 5) shows that, similarly to what was observed for the transformation of HDA into VHDA in pure water, upon compression the first neighbour shell of oxygen remains almost unchanged. Nevertheless in the present case the depth of the minimum at  $\approx 2.9$  Å decreases less markedly than for pure water VHDA, where the second peak becomes a shoulder of the first<sup>45</sup>. The second neighbour shell changes more notably. The position of its maximum moves inwards, from 3.47 Å at ambient pressure to 3.07 Å at 4 GPa. The distribution of O-O-O angles (panel 4 in Figure 5) between first neighbours of the central O, shows that the tetrahedral geometry (single peak at  $\approx 100^\circ$ ), which is still present in the HDA-like phase, is progressively distorted during compression. Above 2 GPa two peaks at 70° and 120° dominate and another peak appears at 180°, this has also been observed in pure water VHDA<sup>46</sup>. The changes of the shell of second neighbours are similar to those observed for VHDA of pure water formed at 3 GPa, where the second neighbours of O are compressed onto the first shell and distorted toward a nearly close-packed structure<sup>46</sup>.

Concerning the hydration of Na<sup>+</sup> ions it can be seen that the second peak in  $g_{ONa}$  at  $\approx 4.5$  Å flattens as pressure increases (relative to the first minimum the peak height drops by 25%), while at the same time the first peak broadens in the 2.5 to 3 Å range. The inward shift of the second peak indicates that the second neighbours have moved closer to the cation. As for the  $g_{OO}$  discussed above this means that the shell of second neighbours is progressively compressed onto the first one and distorted. Accordingly the distribution of the second peak broadens and flattens.

The evolution of average coordination numbers for isothermal compression at 80 K reported in Figure 6 shows that upon densification the shell of first neighbours of sodium ions is more strongly affected than those of oxygen and chlorine. The coordination number of sodium with either chlorine or oxygen (*i.e.*  $N_{NaO} + N_{NaCl}$  using the notation of equation 3) is stable at about 6 up to 2 GPa, which corresponds to octahedral coordination shells. Then it increases nearly linearly with pressure, reaching a value of 6.8 at 7.2 GPa. This is again in contrast to the LiCl case, where the coordination number of lithium with oxygen and chlorine increased step-wise from 4.25 at ambient pressure to 5.1 above 2 GPa.<sup>16</sup> Since Li<sup>+</sup>

<sup>†</sup>  $\rho = 1.35$  g.cm<sup>-3</sup> at ambient pressure and 1.74 g.cm<sup>-3</sup> at 4 GPa in our simulations

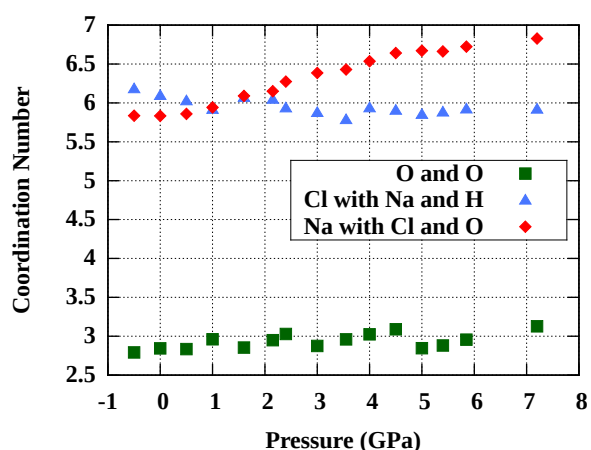


**Fig. 6** Average coordination numbers of oxygen with oxygen (dark green squares), chlorine with sodium and hydrogen (blue triangles), sodium with chlorine and oxygen (red diamonds) under isothermal compression at 80 K. The horizontal axis indicates MD pressure.

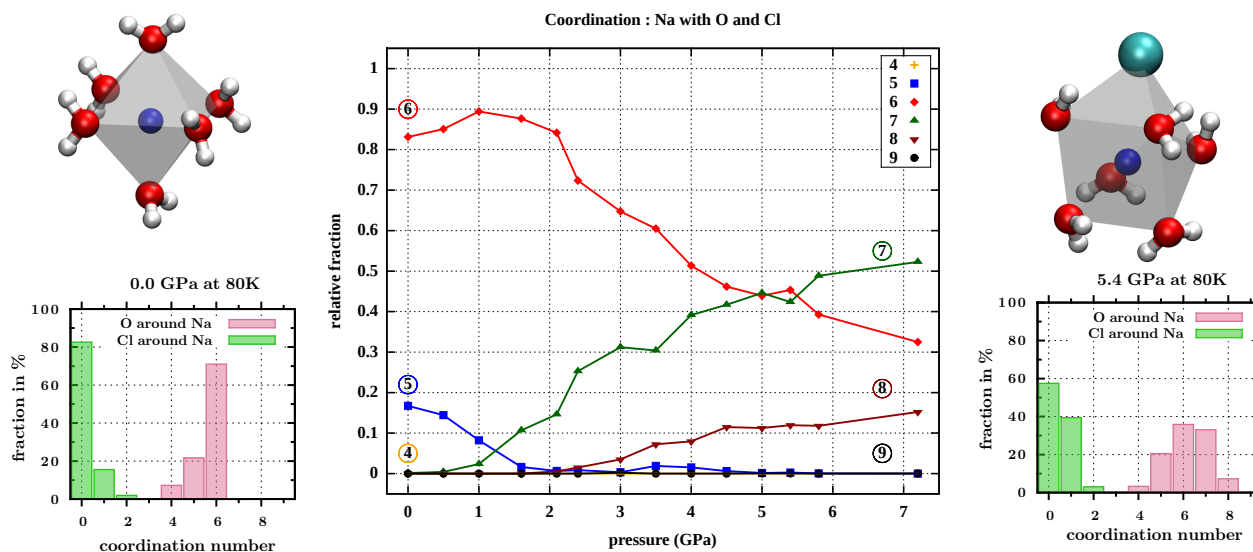


**Fig. 7** Evolution of the distribution of coordination of sodium with oxygen and chlorine for isothermal compression simulated at 80 K (the value of the pressure is that of the simulation). Six distinct populations are shown, the numbers in circles indicate the coordination number of each population. The fraction of 6 fold coordinated atoms decreases, while the fractions of 7 and 8 fold coordinated atoms increase with pressure. The lateral panels show the distribution of  $N_{\text{NaO}}$  and  $N_{\text{NaCl}}$  for the sodium atoms at 0.0 GPa (left) and 5.4 GPa (right), and representations of the local environment of  $\text{Na}^+$  which is octahedral at low pressure and forms an irregular distorted polyhedron at pressures above 4.5 GPa in our simulations.

ions are small ( $r_{\text{Li}^+} = 0.9 \text{ \AA}$ )<sup>47</sup>, they can be fully hydrated by 4 water molecules at ambient pressure. Larger  $\text{Na}^+$  ions ( $r_{\text{Na}^+} = 1.16 \text{ \AA}$ )<sup>47</sup> have octahedral hydration shells at ambient pressure, which are more resilient under compression. The lack of a sudden transition in coordination of the  $\text{Na}^+$  cation is consistent with the absence of a polyamorphic transition. The analysis of the distribution of coordination populations (Figure 7) shows that at pressures below 2 GPa almost all sodium ions remain 6-fold coordinated. Above 5 GPa the dominant population (50 %) is 7-fold coordination, with about 30 % of ions being 6-fold coordinated, and 10 to 15 % being 8-fold coordinated. Finally, the coordination numbers of oxygen with oxygen ( $N_{\text{OO}}$ ) and of chlorine with sodium and hydrogen ( $N_{\text{ClNa}} + N_{\text{ClH}}$ ) are only weakly affected by pressure and remain nearly constant up to 6.5 GPa.

The distribution functions for the first eight neighbours of  $\text{Na}^+$  (Figure 8) show two regimes of compression. In the first one up to 2 GPa, the octahedra are compacted as seen in the distribution of the six nearest neighbours of  $\text{Na}^+$  which move closer toward the center of the octahedron. The first four neighbours, which occupy the region between 2.2 and 2.6  $\text{\AA}$  from the central ion, move inwards by 0.05  $\text{\AA}$ , the fifth by 0.07  $\text{\AA}$  and the sixth by 0.09  $\text{\AA}$ . In the second regime above 2 GPa the first five neighbour peaks broaden but do not shift, the sixth one broadens markedly and shifts outwards slightly. This is consistent with the seventh neighbour moving inward

from a distance of 3.9  $\text{\AA}$  at low pressure to 2.6  $\text{\AA}$  above 2 GPa, thereby distorting the octahedron and eventually breaking it up.<sup>‡</sup> Above 4 GPa the distributions of the first six neighbours do not show appreciable changes; the increase in the 2.6  $\text{\AA}$  peak of the seventh neighbour distribution confirms the increase in coordination.

The changes in the angular distribution functions are consistent with this scenario. Figure 9 shows the distribution of octahedral angles (the angles at the central ion between atoms at the corners of the octahedron), it has one peak near 90° and one near 180°. In the first regime, up to 2 GPa, where the octahedra are compressed, the first peak shifts to smaller angles, from 87° to 82°. Above 2 GPa the first peak does neither shift nor broaden, the second peak broadens noticeably and shifts toward smaller angles ( $\approx 170^\circ$ ), which indicates that the octahedral geometry of the  $\text{Na}^+$  hydration shell is perturbed when the seventh neighbour starts to move inwards. The angles between 100° and 140° are populated above 3 GPa.

## 4 Conclusions

We have found that concentrated NaCl solutions amorphise at ambient pressure in a high density structure similar to

<sup>‡</sup> The eighth neighbour moves inward from 4.1 to 3.4  $\text{\AA}$  and the corresponding peak broadens markedly, but remains largely in the second neighbours shell region.

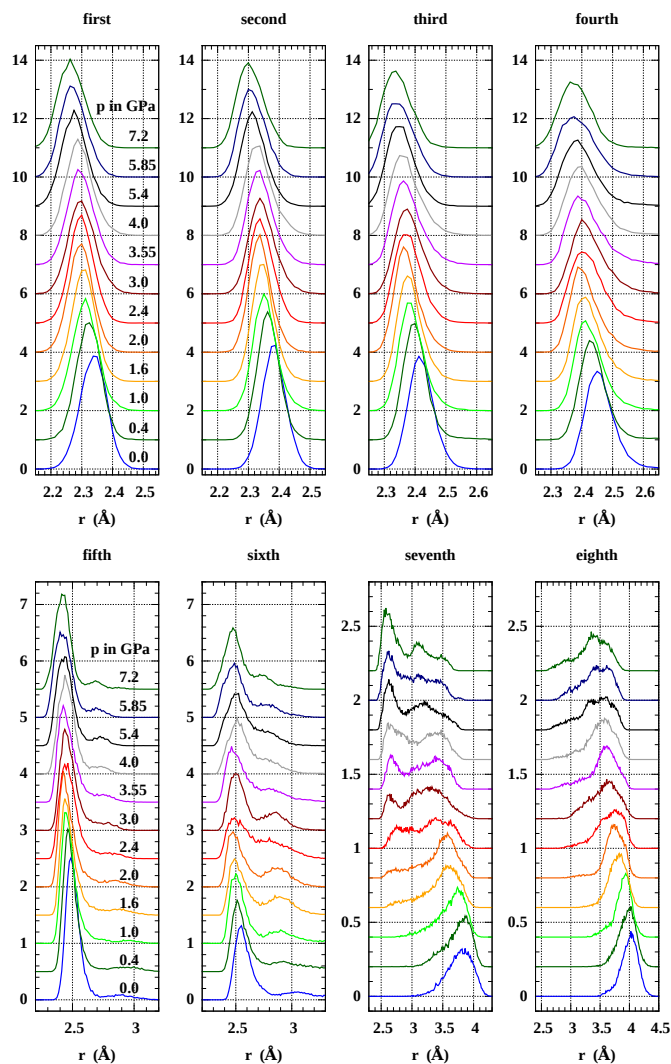


**Fig. 8** Evolution with pressure of distance distribution of eight closest neighbours (O and  $\text{Cl}^-$ ) to  $\text{Na}^+$  ions, where  $r$  is the distance to the sodium ion. The seventh and eighth neighbour move into the shell of first neighbours above 2 GPa.

HDA. The agreement between the structure factors obtained in high pressure neutron diffraction experiments and classical MD simulations using polarizable potentials is remarkably good. Our experimental data suggest that the densification upon compression is a continuous transformation of the amorphous solution, a finding which is supported by our simulations. No evidence for polyamorphism was found, neither under compression nor under annealing at high pressure. This suggests that the polyamorphic phenomenon observed in pure water and aqueous LiCl solutions is not a general feature of electrolytic aqueous solutions. The transition disappears in concentrated NaCl solutions as a consequence of tetrahedral geometry of the water network being distorted by the presence

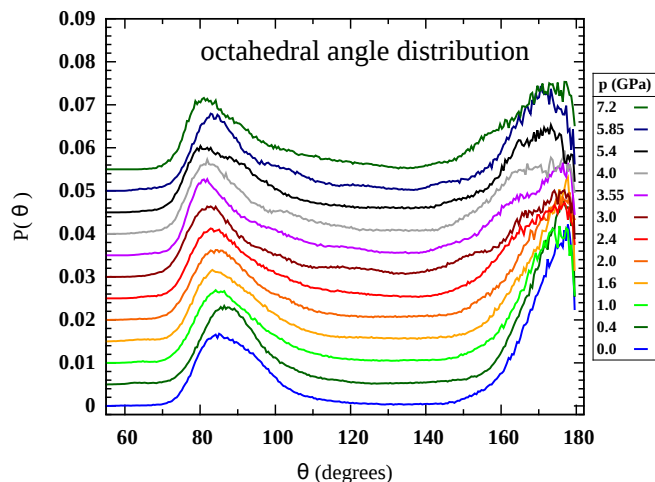


**Fig. 9** Evolution with pressure of the distribution of octahedral angles, which are the angles at the central  $\text{Na}^+$  ion between atoms at the corners of the octahedron formed by the six nearest neighbours.

$\text{Na}^+$  ions.

Densification occurs first by compression of the octahedral coordination shells of  $\text{Na}^+$  ions, followed by a progressive distortion of the octahedra at pressures above 2 GPa. This is in contrast to what was observed in LiCl solutions where  $\text{Li}^+$  shows tetrahedral coordination which abruptly breaks up near 2 GPa, giving rise to a transition to a 6-fold coordinated structure. Given that the structure of ice VII is made of a body centered cubic oxygen lattice, the increase in the fraction of 8-fold coordinated ions with pressure, observed in simulations, suggests that, should NaCl-ice VII crystallize from the dense amorphous phase by further annealing under pressure,  $\text{Na}^+$  ions would most likely occupy a substitutional site in the ice lattice rather than an interstitial one as observed for  $\text{Li}^+$ .<sup>15</sup> Thus the possible existence of substitutional NaCl-ice VII under high pressure deserves further investigation.

## Acknowledgements

We thank J. L. Laborier at Institut Laue Langevin and L. Delbes at IMPMC for technical assistance. We are grateful to R. Pick and S. De Panfilis for fruitful discussions. This work was supported by French state funds managed by the ANR within the Blanc International programme under reference ANR-13-IS04-0006-01 and the Investissements d'Avenir programme under reference ANR-11-IDEX-0004-02, and more specifically within the framework of the Cluster of Excellence MATISSE led by Sorbonne Universités. This work is based on experiments performed at the Institut Laue-Langevin, Grenoble, France and at the ISIS spallation source, Didcot, UK.

## Notes and references

- 1 S. Tazi, J. J. Molina, B. Rotenberg, P. Turq, R. Vuilleumier and M. Salanne, *The Journal of Chemical Physics*, 2012, **136**, 114507.
- 2 C. A. Angell and E. J. Sare, *The Journal of Chemical Physics*, 1970, **52**, 1058.
- 3 H. Kanno, *The Journal of Physical Chemistry*, 1987, **91**, 1967–1971.
- 4 B. Prével, J. F. Jal, J. Dupuy Philon and A. K. Soper, *The Journal of Chemical Physics*, 1995, **103**, 1886–1896.
- 5 G. Neilson and J. Enderby, *Annual Reports Section "C" (Physical Chemistry)*, 1979, **76**, 185–220.
- 6 R. Mancinelli, A. Botti, F. Bruni, M. A. Ricci and A. K. Soper, *Physical Chemistry Chemical Physics*, 2007, **9**, 2959.
- 7 A. Bankura, V. Carnevale and M. L. Klein, *The Journal of Chemical Physics*, 2013, **138**, 014501.
- 8 R. Leberman and A. K. Soper, *Nature*, 1995, **378**, 364–366.
- 9 K. Winkel, M. Seidl, T. Loerting, L. E. Bove, S. Imberti, V. Molinero, F. Bruni, R. Mancinelli and M. A. Ricci, *The Journal of Chemical Physics*, 2011, **134**, 024515.
- 10 P. Ben Ishai, E. Mamontov, J. D. Nickels and A. P. Sokolov, *The Journal of Physical Chemistry B*, 2013, **117**, 7724–7728.
- 11 V. Migliorati, G. Mancini, S. Tatoli, A. Zitolo, A. Filipponi, S. De Panfilis, A. Di Cicco and P. D'Angelo, *Inorganic Chemistry*, 2013, **52**, 1141–1150.
- 12 D. Corradini, P. Gallo and M. Rovere, *The Journal of Chemical Physics*, 2009, **130**, 154511.
- 13 D. Corradini, M. Rovere and P. Gallo, *The Journal of Chemical Physics*, 2010, **132**, 134508.
- 14 L. Le and V. Molinero, *The Journal of Physical Chemistry A*, 2010, **115**, 5900–5907.
- 15 S. Klotz, L. E. Bove, T. Strässle, T. C. Hansen and A. M. Saitta, *Nature Materials*, 2009, **8**, 405–409.
- 16 L. Bove, S. Klotz, J. Philippe and A. Saitta, *Physical Review Letters*, 2011, **106**, 125701.
- 17 G. N. Ruiz, L. E. Bove, H. R. Corti and T. Loerting, *Phys. Chem. Chem. Phys.*, 2014, **16**, 18553–18562.
- 18 J. Dupuy-Philon, J. Jal and B. Prevel, *Journal of Non-Crystalline Solids*, 1992, **150**, 275–280.
- 19 S. Klotz, T. Strässle, R. J. Nelmes, J. S. Loveday, G. Hamel, G. Rouse, B. Canny, J. C. Chervin and A. M. Saitta, *Physical Review Letters*, 2005, **94**, 025506.
- 20 Y. Suzuki and O. Mishima, *Journal of Physics: Condensed Matter*, 2009, **21**, 155105.
- 21 M. R. Frank, C. E. Runge, H. P. Scott, S. J. Maglio, J. Olson, V. B. Prakapenka and G. Shen, *Physics of the Earth and Planetary Interiors*, 2006, **155**, 152–162.
- 22 L. Bezacier, B. Journaux, J.-P. Perrillat, H. Cardon, M. Hanfland and I. Daniel, *The Journal of Chemical Physics*, 2014, **141**, 104505.
- 23 D. Mantegazzi, C. Sanchez-Valle and T. Driesner, *Geochimica et Cosmochimica Acta*, 2013, **121**, 263–290.
- 24 P. Valenti, R. Bodnar and C. Schmidt, *Geochimica et Cosmochimica Acta*, 2012, **92**, 117–128.
- 25 J. Rodriguez-Carvajal, *Physica B: Condensed Matter*, 1993, **192**, 55–69.
- 26 R. J. Nelmes, J. S. Loveday, T. Strässle, C. L. Bull, M. Guthrie, G. Hamel and S. Klotz, *Nature Physics*, 2006, **2**, 414–418.
- 27 A.-A. Ludl, L. E. Bove and S. Klotz, in preparation.
- 28 T. C. Hansen, P. F. Henry, H. E. Fischer, J. Torregrossa and P. Convert, *Measurement Science and Technology*, 2008, **19**, 034001.
- 29 V. F. Petrenko and R. W. Whitworth, *Physics of ice*, Oxford University Press, 1999.
- 30 A. Elarby-Aquizerat, J. F. Jal, C. Ferradou, J. Dupuy, P. Chieux and A. Wright, *The Journal of Physical Chemistry*, 1983, **87**, 4170–4173.
- 31 PEARL website, <http://www.isis.stfc.ac.uk/instruments/pearl>.
- 32 T. Strässle, S. Klotz, K. Kunc, V. Pomjakushin and J. S. White, *Physical Review B*, 2014, **90**, 014101.
- 33 S. Klotz, *Techniques in High Pressure Neutron Scattering*, Taylor & Francis, 2012.
- 34 S. Klotz, G. Hamel, J. Loveday, R. Nelmes and M. Guthrie, *Zeitschrift für Kristallographie*, 2003, **218**, 117–122.
- 35 W. Marshall and S. W. Lovesey, *Theory of thermal neutron scattering: the use of neutrons for the investigation of condensed matter*, Clarendon Press Oxford, 1971.
- 36 CP2K developers group, <http://www.cp2k.org>.
- 37 L. X. Dang and T.-M. Chang, *The Journal of Chemical Physics*, 1997, **106**, 8149–8159.
- 38 A. Aguado and P. A. Madden, *The Journal of Chemical Physics*, 2003, **119**, 7471–7483.
- 39 T. Laino and J. Hutter, *The Journal of Chemical Physics*, 2008, **129**, 074102.
- 40 S. Le Roux and V. Petkov, *Journal of Applied Crystallography*, 2010, **43**, 181–185.
- 41 L. E. Bove, C. Dreyfus, R. Torre and R. M. Pick, *The Journal of Chemical Physics*, 2013, **139**, 044501.
- 42 G. P. Johari, *The Journal of Chemical Physics*, 2005, **122**, 194504.
- 43 E. Whalley, D. D. Klug and Y. P. Handa, *Nature*, 1989, **342**, 782–783.
- 44 O. Mishima, *The Journal of Chemical Physics*, 1994, **100**, 5910–5912.
- 45 J. L. Finney, D. T. Bowron, A. K. Soper, T. Loerting, E. Mayer and A. Hallbrucker, *Physical Review Letters*, 2002, **89**, 205503.
- 46 A. M. Saitta, T. Strässle, G. Rouse, G. Hamel, S. Klotz, R. J. Nelmes and J. S. Loveday, *The Journal of Chemical Physics*, 2004, **121**, 8430–8434.
- 47 R. D. Shannon, *Acta Crystallographica Section A*, 1976, **32**, 751–767.